Macromolecules

Article

pubs.acs.org/Macromolecules

Mesomorphism and Shape-Memory Behavior of Main-Chain Liquid-Crystalline Co-Elastomers: Modulation by the Chemical Composition

Alfonso Ramon García-Márquez,[†] Benoît Heinrich,[†] Nicolas Beyer,[†] Daniel Guillon,[†] and Bertrand Donnio*[,†,‡]

[†]Institut de Physique et de Chimie des Matériaux de Strasbourg (IPCMS), UMR 7504 (CNRS-Université de Strasbourg), 23 Rue du Loess BP 43, 67034 Strasbourg, Cedex 2, France

[‡]Complex Assemblies of Soft Matter Laboratory (COMPASS), UMI 3254 (CNRS-Solvay-University of Pennsylvania), CRTB, 350 George Patterson Boulevard, Bristol, Pennsylvania 19007, United States

Supporting Information

ABSTRACT: The mesomorphic behavior, shape shifting, and shape-memory types of two homologous series of main-chain liquid-crystalline co-elastomers (MC-LCEs) with composition-tunable transition temperatures and mesophases structures are reported. The weakly cross-linked macromolecules were prepared in a one-step procedure by the versatile platinum-catalyzed hydrosilylation reaction between siloxane oligomers (linear spacers and netlike point molecules) and liquid-crystalline binary mixtures, composed of defined proportions of divinylic monomeric mesogens. First, the two sets of alternated, linear copolymers with disiloxane or trisiloxane chain extender, respectively, were investigated. They either exhibit both smectic C (SmC) and nematic (N) phases or a single SmC phase, the nature of which being dictated by the length of the inserted siloxane moieties, and the temperatures ranges regulated by the composition of the mesogenic mixture (mesogens ratio). As anticipated, the thermal behavior of the corresponding co-elastomers is not greatly affected by the weak reticulation (less than 5% w/w), whose transition temperatures (from the ambient to ca. 100 °C) and mesophases types (SmC and N) are quasi-replicated from the polymers and still majority governed by the intermingling of the constitutive components (mesogens ratios, siloxane, and comonomers). Moreover, these MC-LCEs exhibit two types of shape-memory behaviors, which are imposed selectively by the nature of the siloxane extender and which are understood in relation to the mesophases' structures. The combination of small-angle X-ray scattering and thermoelastic experiments gives some fundamental insights into the relationships between molecular structures and macroscopic elastic properties in MC-LCEs in general, which should be beneficial for future designs of soft materials with desired shape-memory properties.

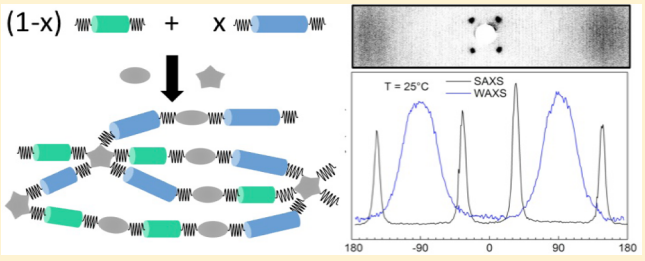

INTRODUCTION

The concept of two-component materials combining at once entropy-induced rubber elasticity and liquid-crystalline ordering was proposed nearly 40 years ago by de Gennes[1] but was not experimentally reached until the successful synthesis in 1981 of the first liquid-crystalline elastomer (LCE) by Finkelmann et al.[2] The exceptional elastic behavior of LCE materials[3,4] and particularly their ability to respond to various external stimuli by significant macroscopic deformations (shape shifting), and to recover their original shape under appropriate excitation (shape memory effect),[5] indeed make them potentially attractive for the implementation into smart materials, including artificial actuators and sensors.[4,6] For instance, LCEs are being successfully integrated in robotics, micro-electromechanical systems (MEMS),[7] systems mimicking muscle performances,[8] and optical grating devices.[9] Micro-actuators have also specifically been developed via soft lithography[10] and microfluidic processes,[11] while cantilevers were obtained by inkjet printing.[12]

Actuation of LCEs essentially relies on the elastic response of the material subjected to an excitation triggered by temperature,[3,4] chemical,[3,4] light,[13] or electric/magnetic fields.[14] In thermally activated systems, the disordering of the low-dimensional liquid-crystalline phase, resulting from the increasing collective molecular movements (mesogens), may lend to large macroscopic deformations of the polymeric network, and the maximum of the amplitude changes usually occurs at the mesophase to isotropic state transformation temperature. Prior to the observation of this remarkable behavior and in order to ensure large actuation amplitudes and stimuli reversibility, the LCE materials need to be macroscopically oriented in the mesophase and must remain stable in this conformation. Large aligned "domains" can be obtained via two-step cross-linking reaction procedures, involving first an intermediate orientation process of the

Received: June 4, 2014
Revised: July 15, 2014
Published: July 24, 2014

   dx.doi.org/10.1021/ma501164u | Macromolecules 2014, 47, 5198−5210

weakly cross-linked gel network by means of a prompt one-dimensional stress. The latter induces a long-range orientation of the mesogens and is kept until the completion of the second reticulation step. Such stable, macroscopically oriented samples are often referred to as "single-liquid crystal elastomers" or as "monodomains".[15]

Current efforts in LCEs focus essentially on (i) developing performing synthetic methods (i.e., facile, reproducible, adaptable), (ii) designing novel macromolecular network topologies,[3,4] and (iii) understanding and fostering predictions of their self-organizing[3,4] and thermoelastic behaviors to define efficient construction strategies for the optimization of these properties.[16,17] Among the great diversity of all the possible network structures realized so far,[3,4] the so-called main-chain LCEs (MC-LCEs)[3,4] have recently generated a lot of interest. Such a macromolecular network is achieved by the weak cross-linking of linear polymeric chains, whose anisotropic pro-mesogenic moieties are inserted in the polymer backbone. Because of the intrinsic linear topology, these LCEs exhibit extraordinary elastic properties, such as high conformational anisotropy, high orientability, and large strain amplitudes, which arise precisely from the direct coupling between the long-range liquid-crystalline order (from the mesogens) and the polymer chain network conformation.[3,4] Main-chain systems are therefore extremely appealing when strong deformations, long cyclic actions, and high sensitivity to thermal stimuli are required.

From a more fundamental point of view, the systematic development of a wide range of MC-LCEs, integrating an unrestricted variety of pro-mesogens, spacers, and cross-linkers, is propitious to the better understanding of their intimate structure−activity relationships as well as essential to the investigation of theoretical models of their thermal-induced elastic behaviors in the mesophases and in the isotropic phase.[16,18] In this respect, comblike LCEs (with mesogenic side groups pending from the linear chains) have been widely studied due to their relatively straightforward and accessible syntheses.[3,4] In contrast, such investigations are however only emerging for MC-LCEs,[4] consequently to numerous synthetic difficulties encountered during their preparation (e.g., arduous isolation of precursory linear polymers, low coupling, and cross-linking efficiencies as reflected by high soluble contents, low control of the network density, and low synthetic reproducibility) and inadequate physicochemical properties (low solubility, high transition temperatures, low thermal stability, high propensity to form stiff solids, and rigid polydomain materials), prejudicial to conduct reproducible measurements.[19−24] Aiming at improving the quality and accessibility of MC-LCEs, several elegant synthetic approaches are currently being explored, which include the photo-cross-linking of main-chain prepolymers (laterally functionalized by photo-cross-linkable units[25] or with the photo-cross-linkable units inserted within the polymer backbone[26]), the photoinduced addition of thiols on olefins (aka thiol−ene photopolymerization) of monomers containing olefinic and mercapto end-groups,[27] or the thermally activated cross-linking of end-unsaturated polymers.[28] Also, and of specific interest in this study, is the "one-pot" approach,[29] solely based on the chemistry of linear siloxane-containing LC polymers.[30] This highly versatile synthetic methodology (vide supra) consists of the hydrosilylation of divinylic liquid-crystalline monomers with linear and cyclic siloxane comonomers, as chain-extender and reticulating group, respectively, allowing therefore both chain propagation and reticulation to occur simultaneously. All these new methods generally permit the preparation of macroscopically aligned thin elastomeric films as well as improve their processing by novel techniques such as electrospinning,[25] replica molding,[27] and the enhancement of the anisotropic factor via chemical approaches,[31] swelling-induced electro-optical effect,[32] and piezoelectric and mechanical effects.[24,31]

Elastomers represent also an interesting class of stimuli-responsive materials as they are intrinsically shape-memory materials due to the hindered chain' reptation[33,34] mandated by the reticulation. Essentially two types of shape memory effects have been described in the literature for polymers. The one-way type situation is commonly observed in amorphous polymers.[5] Such a mode consists in the recovery of the initial "primary" shape on heating, starting from an elongated "secondary" shape, beforehand obtained at low-temperature upon a mechanical stress. Lowering the temperature again, the primary shape is conserved until the application of a subsequent mechanical stress. This type is quite different from the second-way memory shape effect, which consists in the continuous and reversible shape-shift between two thermodynamically stable states. Both types of shape memory effects occur in LCEs,[5] but the second mode is more specific for nematic LCEs,[35] since very different elongation amplitudes are generated by the large variations of the order parameter with temperature (the cross-linking hinders thermal motions of the mesogens but hardly the thermal fluctuations of their main common orientation). This variation is continuous and reversible[36] between the most elongated status close to the bottom limit of the N domain and the maximum shrinking status, in the paranematic state, above the smeared off transition (vide infra).[5]

RESULTS AND DISCUSSION

Design. In this competitive and stimulating context, we therefore endeavored the synthesis and characterization of two series of weakly cross-linked mesomorphous MC-co-elastomers showing a N phase by employing a combination of various chemical approaches, including (i) the "one-pot" hydrosilylation of divinylic liquid-crystalline monomers with linear and cyclic siloxane comonomers, as chain-extender and reticulating group, respectively;[29] (ii) the introduction of precise binary mixtures of mesogenic monomers, [$\mathbf{N1}_x$ + $\mathbf{N2}_{1-x}$], **N1** showing individually a nematic phase (N) and **N2** a smectic C phase (SmC) over different temperature ranges, in order to reduce mesophase symmetries and to lower transition temperatures; (iii) the insertion of the siloxane fragments of different length between mesogens, **TMDS** or **HTMS**, to yield soft materials, with low transition temperatures; (iv) the synthesis of mesogenic monomers bearing end-vinyl−ether functional groups to enhance reactivity and thus to reduce soluble contents;[37,38] and finally (v) the use of a 5-fold cross-linker, **HD5**, to ensure the formation of the network.[31] Such a design was elaborated in order to accurately investigate the relationships between the mesophase structures and the shape shifting and memory-shape behaviors of the elastomers.

The versatility of this methodology has been largely demonstrated since it was first reported, and a large number of siloxane-based MC-LCEs have been prepared accordingly, merely requiring the preparation of customized divinylic-terminated mesogens.[29,31] This straightforward approach indeed presents several advantages: (i) it permits the readily achievement of thermally stable MC-LCEs with low phase-transition temperatures due to the regular alternation of

dx.doi.org/10.1021/ma501164u | Macromolecules 2014, 47, 5198−5210

Scheme 1. Synthetic Routes for the Monomers N1 and N2 (Intermediate Yields)[a]

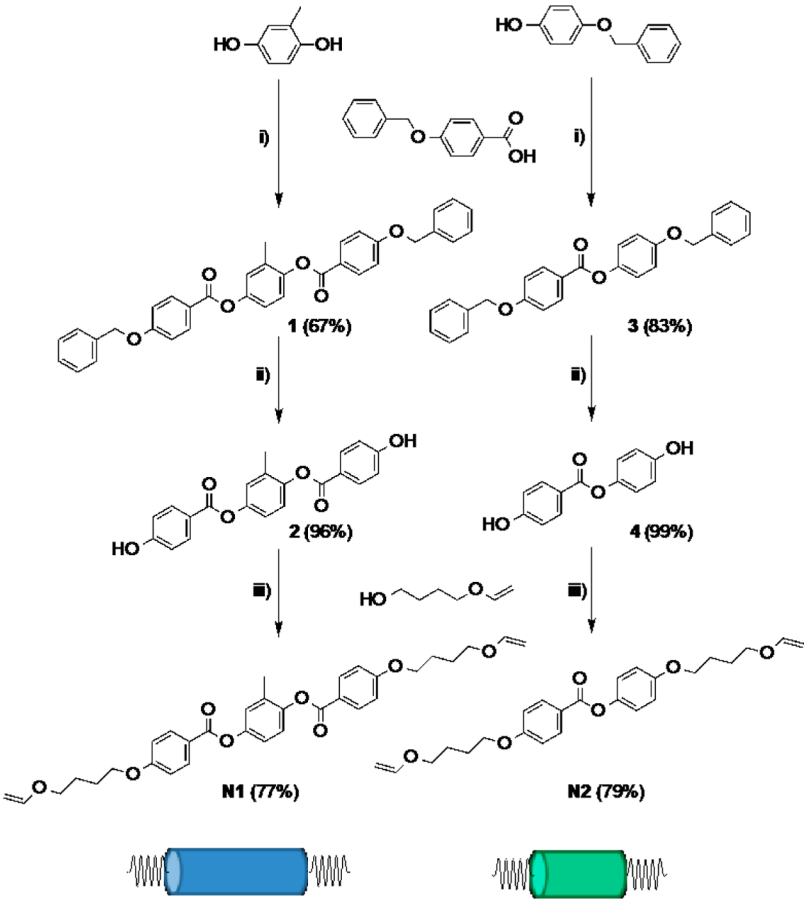

[a]The detailed synthetic procedures are given in the Supporting Information: (i) DMAP, EDCI·HCl, CH_2Cl_2, 0 °C, 5−12 h; (ii) Pd/C (10%), H_2, THF, rt, 5−6 h; (iii) DIAD, PPh_3, THF, 0 °C for 1 h and rt for 8 h.

siloxane and mesogenic units within the polymeric backbone, (ii) offers the access to a wide range of macromolecular structures consequently to the incorporation of the individual constituents with unrestricted molecular shapes, and (iii) allows straight and subtle modifications of the MC-LCEs structures by easy permutations of the various components and modifications of their respective proportions. Such flexibility in the choice of the individual components is very unique and should in principle permit complete systematic structure−activity investigations to tune the desired ultimate physical properties. A recent improvement of the synthesis has just consisted in considering LC monomers bearing vinyl−ether functional end-groups, which considerably enhances the efficiency of the hydrosylilation addition, as evidenced by lower soluble contents determined in the corresponding MC-LCEs.[37,38]

The self-organizing and thermal behaviors of the two sets of weakly cross-linked LCEs and of their related linear polymers have been comprehensively examined by the combination of POM (polarized-light optical microscopy), DSC (differential scanning calorimetry), and SAXS (small-angle X-ray scattering) techniques. Preliminary results of the thermoelastic behavior of four representative LCEs have also been briefly described and their elastic performances tentatively rationalized with the mesophases' structures.

Monomers and Mixtures. In this study, two commonly used mesogenic monomers were considered, **N1**[37] and **N2**,[38] that principally differentiate by their core lengths and by the presence of a lateral methyl group in one case (Scheme 1). The synthetic route used for their preparation was performed in three successive high-yield steps (Scheme 1, detailed procedures in Supporting Information), starting with the esterification of methylhydroquinone and 4-benzyloxyphenol with 4-(benzyloxy)benzoic acid (Scheme 1, **1** and **3**, respectively), followed by the removal of the protecting benzyl pending groups via catalytic hydrogenation (Scheme 1, **2** and **4**) and by the subsequent binding of 4-vinyloxybutan-1-ol fragments to the rigid cores **2** and **4** by the standard Mitsunobu etherification. The overall yields after purification were 50 and 65% for **N1** and **N2**, respectively. Three binary mixtures [$\mathbf{N1}_x$ + $\mathbf{N2}_{1-x}$] were prepared with molar ratios x:(1 − x) = 0.25:0.75, 0.50:0.50, and 0.75:0.25 by dissolving the appropriate quantities of each monomer in dry dichloromethane, followed by slow solvent evaporation and vacuum drying (Supporting Information).

As clearly identified by POM (Figure S4, Supporting Information), **N1** presents a N phase over a broad temperature range (Cr 82 N 168 I),[37] while the shorter **N2** presents a SmC phase over a small temperature interval (Cr 72 SmC 87 I).[38] The long mesogen **N1** logically leads to the broader liquid-crystalline range (N), whereas the smectic phase vanishes in the presence of the methyl group while perturbing the lateral packing in layers.[39] These two compounds are not miscible in the crystalline state and likely form eutectic systems, but after several heating−cooling cycles, the various mixtures behave

dx.doi.org/10.1021/ma501164u | Macromolecules 2014, 47, 5198−5210

homogeneously as indicated by reproducible DSC traces (Figure S8, Supporting Information). The smectic phase already vanishes with the lowest **N1** added concentration, and all the mixtures show a broad N range, induced at intermediate compositions by the melting temperature depression and the linear variation of the clearing temperatures (Figure 1 and Table S10, Supporting Information). Among the

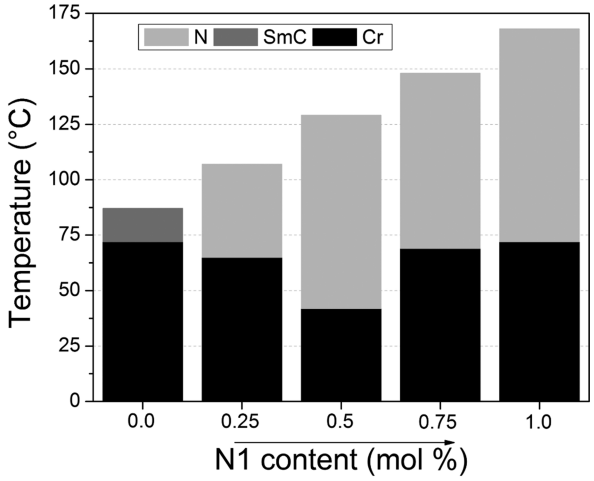

Figure 1. Comparative phase diagram of the monomers **N1** and **N2** and their three binary mixtures $[\mathbf{N1}_x + \mathbf{N2}_{1-x}]$ (x = 0.25, 0.50, and 0.75) as a function temperature. N, nematic phase; SmC, smectic C phase; Cr, crystalline phases (Table S10, Supporting Information).

binary mixtures, the largest N temperature range is observed for the equimolar mixture $[\mathbf{N1}_{0.50} + \mathbf{N2}_{0.50}]$ also having the lowest melting transition temperature.

Main-Chain (Co)polymers. Two series of homogeneous main-chain liquid-crystalline copolymers, alternating siloxane fragments of different length, i.e. 1,1,3,3-tetramethyldisiloxane (**TMDS**) or 1,1,3,3,5,5-hexamethyltrisiloxane (**HMTS**), with mesogens **N1** and **N2**, were then prepared (Scheme 2). In this study, the polymers need to be synthesized with high polymerization degrees (p), as they are the reference materials of elastomers to be potentially compatible with actuating applications, thus based on the interconnection of long

Scheme 2. Sketched Illustration of the Synthesis of the Two Series of Linear Polymers with Different Mesogenic Monomer Ratios and Oligosiloxane Spacers ($[\mathbf{N1}_x + \mathbf{N2}_{1-x} + \mathbf{TMDS}]_p$ and $[\mathbf{N1}_x + \mathbf{N2}_{1-x} + \mathbf{HMTS}]_p$)[a]

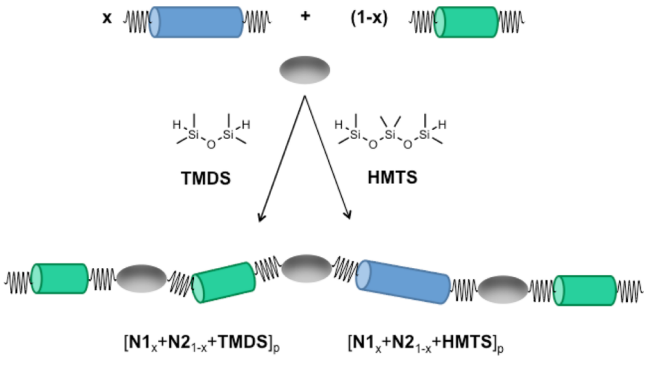

[a]Reaction conditions: toluene, $PtCl_2COD$, 60 °C, 24 h (see details in Supporting Information).

polymeric chains. Moreover, to compare polymers and elastomers, the polyaddition reactions were performed in the same highly concentrated conditions as those used for the synthesis of the elastomers described in the next section. They were obtained by platinum-catalyzed hydrosilylation in toluene between equivalent proportions of siloxane comonomers (**TMDS** or **HMTS**) as chain spacers and the appropriate mixtures of mesogens $[\mathbf{N1}_x + \mathbf{N2}_{1-x}]$ in different proportions (Scheme 2, thereafter the polymers will be abbreviated as $[\mathbf{N1}_x + \mathbf{N2}_{1-x}\text{+}\mathbf{TMDS}]_p$ and $[\mathbf{N1}_x + \mathbf{N2}_{1-x}\text{+}\mathbf{HMTS}]_p$, respectively; Tables S1 and S2, Supporting Information).

All polymers and copolymers were purified via coprecipitation (THF/MeOH) and the molecular weights analyzed by gel permeation chromatography (GPC, Tables S3 and S4, Supporting Information). Average degrees of polymerization ranging from 40 to 245 units were obtained, with acceptable to high polydispersity indices (PDI), comprised between 2.0 and 7.0 (PDI = M_w/M_n), most of them in the expected range for such polyaddition reactions;[30] the best results were found for the **TMDS** systems. ^{1}H NMR helped to confirm the retention of the initial ratios of monomers after polymerization, by comparing the total Si−CH_2 integration with that of the methyl signals from the **N1** moiety (Table S5 and Figure S1, Supporting Information).[40]

The structural features, common to all synthesized polymers, are both (i) the presence of fairly long decoupling spacers between consecutive mesogens conferring an alternated polymeric structure[30] and (ii) the existence of constitutional regio-inhomogeneity caused by the random orientations and distributions of the two mesogenic groups along the polymer backbone, beneficial for the decrease of the lateral interactions and thus to foster low transition temperatures (both monomers are noncentrosymmetrical due to the presence of the lateral methyl group in the central ring of **N1** and to the polar ester bond between the two aromatic rings in **N2**). As inferred by POM (Figures S5 and S6, Supporting Information), DSC (Figure S9, Figure S10, and Table S11, Supporting Information), and SAXS (Figure S13, Supporting Information), all the linear polymers exhibit thermotropic liquid-crystalline behavior from room temperature up to ca. 100 °C. The overall phase behavior of both series of polymers can be summarized as displayed in the diagram below (Figure 2).

All the **N1**-containing polymers of the **TMDS** series exhibit two mesophases, assigned to as SmC and N phases; the **N2**-homopolymer, previously reported elsewhere, is deprived of the N phase but exhibits instead an additional unidentified phase below the SmC phase.[38] Apart from the transition peaks, the DSC traces of the **TMDS** copolymers (Figure S9, Supporting Information) also contain a specific heat jump around −20 ± 5 °C, attributed to the glass transition (T_g). While T_g is rather insensitive to the binary composition, the clearing temperature steadily increases with the **N1** content, at a comparable rate as in the monomeric mixtures, but with a lowering of about 60 °C. The main difference with respect to the monomers and mixtures consists in the induction of a SmC phase throughout the series, below a transition temperature, also quasi-invariant with composition. This phase is then retained down to room temperature, replacing the crystalline range of the monomers.

In contrast, the N phase has totally vanished in the polymers of the **HMTS** series, for which a direct transition from the SmC phase to the isotropic state is observed (Figure S10, Supporting Information). Clearing temperatures lie between the SmC-N and the N−I phases' transitions of the **TMDS** polymers,

dx.doi.org/10.1021/ma501164u | Macromolecules 2014, 47, 5198−5210

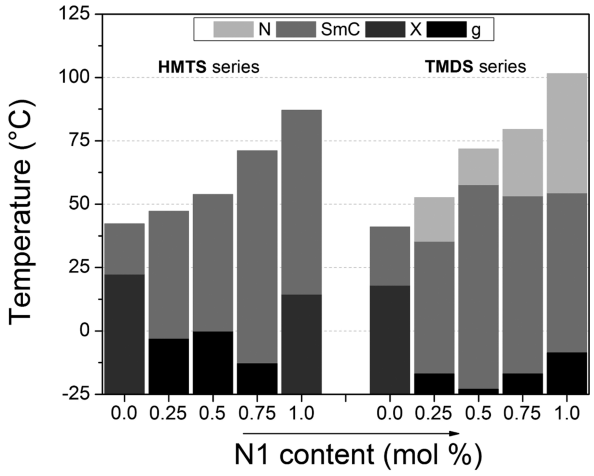

Figure 2. Comparative phase diagram of both series of copolymers, $[\mathbf{N1}_x + \mathbf{N2}_{1-x} + \mathbf{HMTS}]_p$ and $[\mathbf{N1}_x + \mathbf{N2}_{1-x} + \mathbf{TMDS}]_p$, as a function of the **N1** content (mol %) and temperature. N, nematic phase; SmC, smectic C phase; g, glassy state; X, unidentified phase. **TMDS** homopolymers (x = 0, 1) were not made in this work, but transition temperatures were taken from literature for comparison (refs 37 and 38).

therefore increasing with the **N1** content (Figure 2). Glass transitions are observed for two copolymers only, namely $[\mathbf{N1}_{0.50} + \mathbf{N2}_{0.50} + \mathbf{HMTS}]_p$ and $[\mathbf{N1}_{0.75} + \mathbf{N2}_{0.25} + \mathbf{HMTS}]_p$ (T_g = −20 and −13 °C, respectively); the other terms of the series exhibit an additional phase, slightly below room temperature, which could not be further investigated (thereafter referred to as X).

SAXS patterns confirm in all cases the SmC structure of the mesophase: they contain diffuse halos in the wide-angle region, occurring from liquidlike lateral distances within sublayers, and a sharp reflection in the small-angle region with a periodicity compatible with tilted layers (Table 1 and Figure S13, Supporting Information).

The halo at around 6.3−6.6 Å was readily assigned to the siloxane sublayers (h_{si}), while the maximum at 4.6−4.8 Å overlaps the scattering signals from distances between molten aliphatic chains (h_{ch}) and mesogens (h_{mes}), respectively. The SmC periodicities lie in the same range and only vary little from one series to another, e.g., 28 ± 0.5 Å within the **TMDS** series and 29 ± 0.7 Å within the **HMTS** series. The patterns recorded in the N phase of the **N1**-containing **TMDS** polymers are similar to the ones in the smectic phase, apart from the trivial broadening of the small-angle reflection. The correlation length, associated with this broad feature, lies in the range of about 3 nm (Scherrer formula); that is, it extends to first neighbor's interactions. In the wide-angle region, the patterns contain an unresolved broad scattering with a maximum around 5.0−5.5 Å, overlapping the signals of h_{si}, h_{ch}, and h_{mes}.

Thus, as anticipated, all the alternated polymers resulting from the combination of siloxane and mesogenic moieties are mesomorphic, exhibiting SmC or SmC and N phases.[30] Although their clearing temperatures are considerably below the corresponding monomeric mixtures, the introduction of the flexible siloxane segments widens the mesomorphic ranges to room temperature. The siloxane spacers moreover induce the formation of the smectic phase, systematically present, and extending to higher temperatures with the longer spacer, while the N range shrinks in **TMDS** polymers or vanishes totally in **HTMS** polymers. This trend is just the inevitable consequence

Table 1. Structural Data of the Disiloxane (SmC and N) and of the Trisiloxane (SmC) Polymers and Copolymers, $[\mathbf{N1}_x + \mathbf{N2}_{1-x} + \mathbf{TMDS}]_p$ and $[\mathbf{N1}_x + \mathbf{N2}_{1-x} + \mathbf{HMTS}]_p$[a]

polymers	mesophase	d	h_{si}	$h_{mes} + h_{ch}$
$[\mathbf{N1}_{0.25} + \mathbf{N2}_{0.75} + \mathbf{TMDS}]_p$	SmC N	27.6 ca. 30	6.5 ca. 5.0−5.5	4.5 ca. 5.0−5.5
$[\mathbf{N1}_{0.50} + \mathbf{N2}_{0.50} + \mathbf{TMDS}]_p$	SmC N	27.6 ca. 30	6.6 ca. 5.0−5.5	4.5 ca. 5.0−5.5
$[\mathbf{N1}_{0.75} + \mathbf{N2}_{0.25} + \mathbf{TMDS}]_p$	SmC N	28.5 ca. 30	6.6 ca. 5.0−5.5	4.7 ca. 5.0−5.5
$[\mathbf{N2} + \mathbf{HMTS}]_p$	SmC	28.3	6.5	4.6
$[\mathbf{N1}_{0.25} + \mathbf{N2}_{0.75} + \mathbf{HMTS}]_p$	SmC	28.6	6.5	4.6
$[\mathbf{N1}_{0.50} + \mathbf{N2}_{0.50} + \mathbf{HMTS}]_p$	SmC	28.5	6.8	4.7
$[\mathbf{N1}_{0.75} + \mathbf{N2}_{0.25} + \mathbf{HMTS}]_p$	SmC	29.0	6.6	4.7
$[\mathbf{N1} + \mathbf{HMTS}]_p$	SmC	29.7	6.6	4.8

[a]Abbreviations: SmC, smectic C mesophase; N, nematic phase. Structural data measured at 25 °C for SmC phase and at 50, 64, and 68 °C in the N phase (with increasing **N1** content): d, h_{si}, h_{mes}, h_{ch}: layer spacing and scattering maxima for lateral distances between siloxane fragments, mesogenic monomers, and aliphatic chains, respectively (all distances are given in Å).

of the nanosegregation of the siloxane moieties.[30,41] The intercalation of the siloxane sublayers logically guarantees the formation of overall long-range correlated layers but also reduces interactions between successive mesogen-containing strata and thus leads to the early vanishing of the long-range correlated orientational order above the smectic range. The impact on the mesomorphism is straightforward and less important for the shorter spacer (**TMDS** series) and still competes with the deleterious effect of the lateral methyl group borne by the **N1** mesogen (vide infra in **TMDS** elastomers), resulting in their shrunken N ranges. In the **HMTS** series, the mesomorphism is clearly dominated by the smectic phase and the nanosegregation of the siloxane spacers.

Main-Chain (Co)-Elastomers. The synthesis of the main-chain co-elastomers (Scheme 3) was performed according to the previously described one-pot synthesis[29,31] in a custom-build centrifuge (Figures S17 and S19, Supporting Information). The following protocol was kept identical for all systems: the binary mixture of mesogenic monomers ($\mathbf{N1}_x + \mathbf{N2}_{1-x}$), the spacer (**HMTS** or **TMDS**), and the 5-fold cross-linker (2,4,6,8,10-pentamethyl-1,3,5,7,9,2,4,6,8,10-pentaoxapentasilecane, **HD5**) were combined in a small 5 mL vial in adequate proportions (Tables S6 and S7, Supporting Information), dissolved in ca. 0.9−1 mL of freshly distilled toluene, and the mixture heated gently to 60 °C until complete dissolution; in all cases, the proportion of cross-linker **HD5** was kept constant throughout the entire series of compounds, i.e., 4−5 mol % (e.g., 0.1 equiv/mmol). The catalyst was then added, and the reaction mixture introduced in the customized cell, which was then hermetically sealed. The mixture was left to react for 10 min, before centrifugation was started (60 °C, 1−3 h, 3000 rpm).

Well-aligned elastomeric thin films were prepared via the standard two-step method due to the flexibility introduced by the siloxane segments (Figure S2, Supporting Information).[29,31] The resulting fragile strips of gels were carefully removed from

dx.doi.org/10.1021/ma501164u | Macromolecules 2014, 47, 5198−5210

Scheme 3. Sketched Illustration of the Synthesis of the Two Series of Main-Chain Co-Elastomers ([$N1_x$ + $N2_{1-x}$ + TMDS +HD5] and [$N1_x$ + $N2_{1-x}$ + HMTS + HD5]) with Different Mesogenic Monomer Ratios and Oligosiloxane Spacers[a]

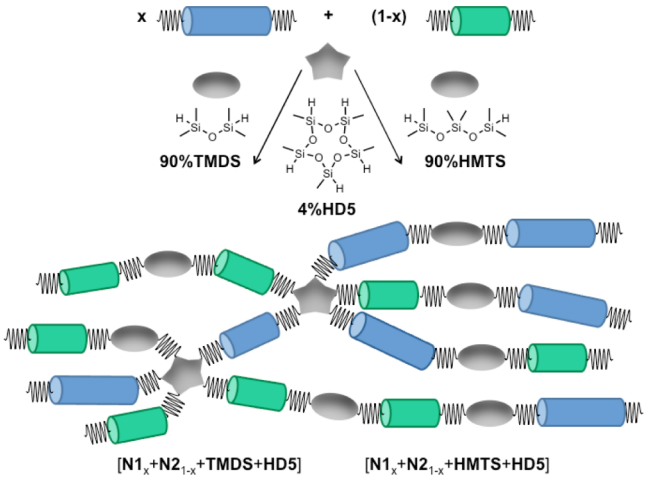

[a]Reaction conditions: toluene, $PtCl_2COD$, 60 °C, 1−3 h, 3000 rpm.

the centrifuge cell, previously cooled down to room temperature to lower reaction rate, and various rectangular lumps of the elastomer were hung at one extremity. One-dimensional alignment, e.g. parallel to the long strip axis, was achieved by loading the other end with weights (a few milligrams) until the liquid crystalline gel changed from turbid to transparent. The films were then dried at 60 °C for 3 days and cooled down to room temperature while still strained with the load. The removal of the load lefts the elongated shape of the material unchanged, likely because of the presence of the room temperature LC phase (SmC). As evidenced previously,[31] the deformation from the initial shape preceding the orientation process can be frozen into a "secondary" shape by crossing the transition toward the smectic phase. Remarkably, this process is purely due to mesomorphism and occurs for elastomers with subambient glass transitions and therefore soft textures (like the compounds studied here), in contrast to most of the shape-memory polymer networks of the other types.[5a] The secondary shape of smectic elastomers may remain unchanged after several years aging.[37]

The completion of the alignment procedure consists in washing the elastomers in a suitable solvent and extracting the soluble content (sol %, corresponding to soluble part embedded in the network) by means of successive Soxhlet extractions in cyclohexane. A high soluble content yields poor cross-linked, mechanically fragile networks. Hence, the lower the soluble content, the better the quality of the material. Here, the soluble contents determined were rather low, varying from 25 to 3% (Figure S3, Supporting Information), and are comparable to the previously best reported siloxane-containing elastomers.[31,32] Swelling experiments were carried out in toluene at 25 °C (Figure S3, Table S8, and Table S9, Supporting Information). The co-elastomer samples presented different dimensional changes in parallel ($\alpha_{\parallel}$) or perpendicular ($\alpha_{\perp}$) with the direction of the applied stress during the orientation process. The alignment of the cross-linked polymer chains should reduce the swelling along the stress direction, in accordance with high swelling anisotropies found for the elastomers of both series ($q_z = \alpha_{\perp}/\alpha_{\parallel}$, the swelling anisotropy, is the ratio between the film dimensions before and after toluene infiltration). Surprisingly, the homoelastomers of the **HMTS** series do not follow this expected behavior and swell in an almost "isotropic" way.

The thermal behavior of both series of elastomers was mainly characterized by DSC and SAXS; POM studies revealed changes in the luminosity of the samples, but without characteristic textures, providing information about the nature of the mesophases formed, but not their complete elucidation. Nevertheless, the high initial birefringence suddenly vanishes at the temperature of the highest DSC peak, when the elastomers transform into the isotropic-like state (Figure S7, Supporting Information). Overall, the trend observed for the polymers (Figure 2) can be translated to the corresponding elastomers (Figure 3), evidencing that a low cross-linking density does not affect greatly the thermal behavior.

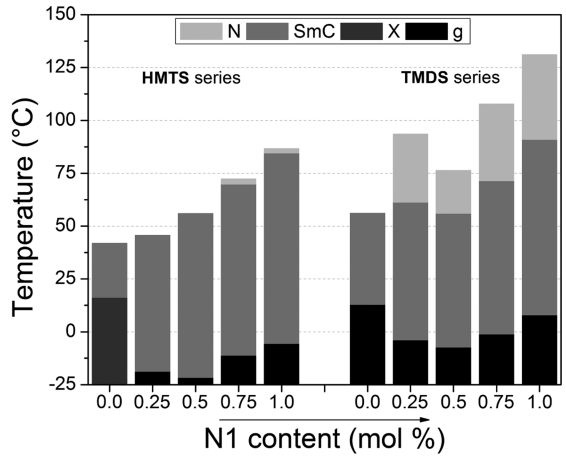

Figure 3. Comparative phase diagram behavior of both series of co-elastomers ([$N1_x$ + $N2_{1-x}$ + **HMTS** + **HD5**] and [$N1_x$ + $N2_{1-x}$ + **TMDS** + **HD5**]) as a function of the **N1** content (mol %) and temperature (°C). N, nematic phase; SmC, smectic C phase; X, unidentified phase; g, glassy state. **TMDS** homoelastomers (x = 0, 1) were not made in this work, but transition temperatures were taken from literature for comparison (refs 37 and 38).

The elastomers of the **TMDS** series show the same sequence of states as the corresponding polymers, except that the transition temperatures are substantially increased: T_g is increased by roughly 15 °C, the SmC to N transition by about 20 °C, and the N to isotropic state (actually paranematic-like state, I_N, vide supra) by on average 25 °C (Figure S11 and Table S12, Supporting Information). On the contrary, the thermal behavior of the **HMTS** elastomers is almost the carbon copy to that of the corresponding polymers: they show at almost the same temperatures, the SmC phase, the glassy state, or a subambient unidentified phase "X" (Figure S12 and Table S12, Supporting Information). The only significant difference consists in the appearance of an additional mesophase above the SmC phase, likely a N phase, for the materials with the highest **N1** contents (for $x \geq 0.5$). Although the mesophase temperature range is too narrow (a few degrees) for a definitive confirmation by SAXS, the reappearance of the N phase could be explained by the slightly thinner siloxane sublayers as compared to that of the polymers and also possibly to the partial disordering of the smectic layers upon the introduction of the disturbing cross-linker (vide infra).

SAXS patterns of all co-elastomers are consistent with aligned SmC materials, as they contain diffuse bows centered

dx.doi.org/10.1021/ma501164u | Macromolecules 2014, 47, 5198−5210

on the equatorial plane for the scattering maxima h_{Si}, h_{ch}, and h_{mes} and a set of four small-angle Bragg spots revealing the cone distribution of the lamellar first-order reflection around the elongation direction, parallel to the meridian (Figures 4 and 5,

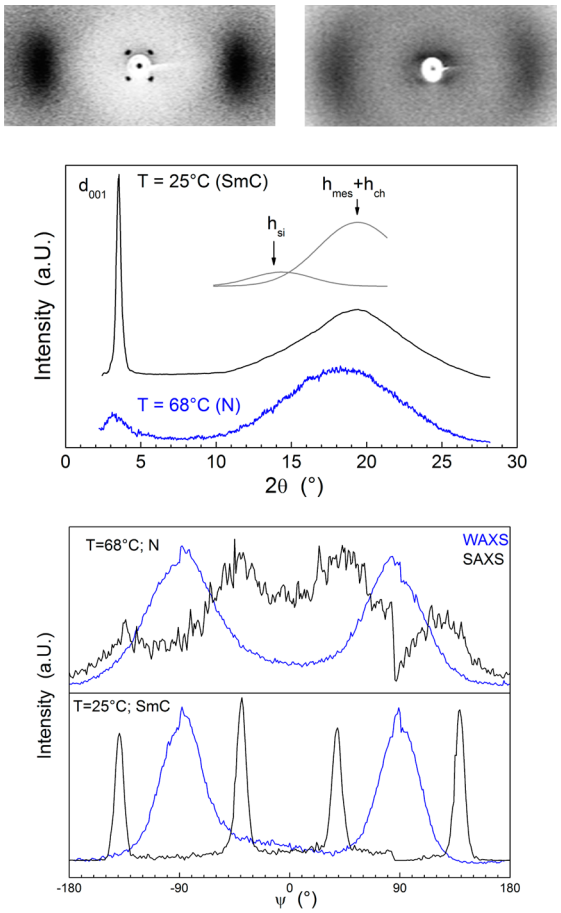

Figure 4. X-ray data of co-elastomer [$\mathbf{N1}_{0.50}$ + $\mathbf{N2}_{0.50}$ + **TMDS** + **HD5**], chosen as a representative example. Top: aligned SAXS patterns in the SmC phase at 25 °C, left, and in the N phase at 68 °C, right (the direction of elongation is parallel to the meridian); middle: radial profiles over 360° of the corresponding mesophases (d_{001}, h_{si}, h_{mes} + h_{ch}: first-order lamellar periodicity, and scattering maxima for lateral distances between siloxane units, monomers, and chains; bottom: azimuthal profiles of both mesophase in the wide- and small-angle regions (the direction of elongation corresponds to ψ = 0, ±180°).

Table 2, Figures S14 and S15, Supporting Information). The layer spacings of the **TMDS** (25.5 ± 1.0 Å) and **HMTS** (28 ± 1.0 Å) elastomers SmC phases are slightly reduced with respect to the periodicities of the SmC phases of the corresponding polymers (by about 2 and 1 Å, respectively); therefore, the mesogens are slightly more tilted, mainly due to the expansion of the cross-linkers within the siloxane sublayers. When **TMDS** elastomers are heated in the N phase, the only important change in the SAXS patterns consists in the widening of the small-angle spots, the alignment remaining almost the same. This widening is however limited, and corresponds to correlation lengths of about 4 times those found for the **TMDS** polymers, amounting to clusters of 4−5 neighboring layers. Comparable large positional correlations have been previously found in the N phase of other related main-chain elastomers.[38]

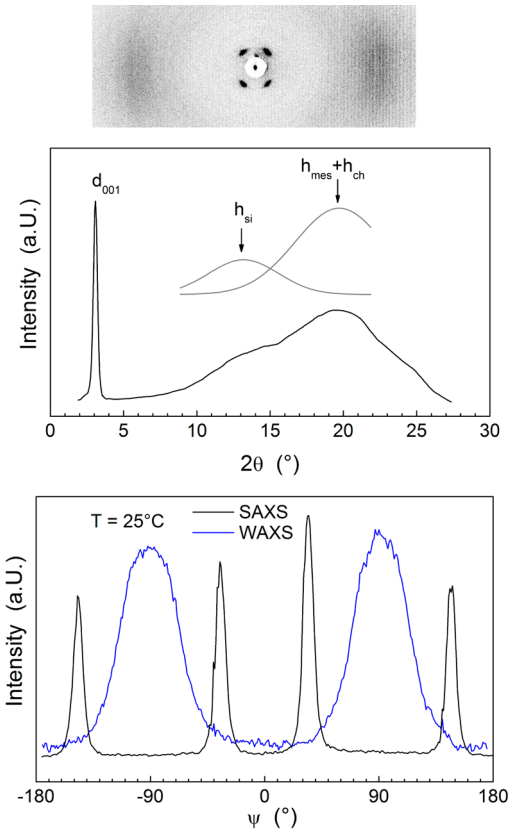

Figure 5. X-ray data of co-elastomer [$\mathbf{N1}_{0.50}$ + $\mathbf{N2}_{0.50}$ + **HMTS** + **HD5**], chosen as a representative example. Top: aligned SAXS pattern in the SmC phase at 25 °C (the direction of elongation is parallel to the meridian); middle: radial profiles over 360°; bottom: azimuthal profiles in the wide- and small-angle regions (the direction of elongation corresponds to ψ = 0, ±180°).

When the isotropic state (or paranematic-like, vide supra) is reached, the small- and wide-angle scatterings blur out the broad halos. Residual orientations can however be detected for the **TMDS** elastomers only, but this peculiar behavior only comes in the forefront on cooling in the mesophase: the elastomers of this series reproduce similar oriented patterns than on heating, while the elastomers of the **HMTS** series give rise to patterns with continuous rings, probing the isotropically oriented smectic domains. A deeper insight in the recovery process of the **TMDS** elastomers was deduced from SAXS patterns of [$\mathbf{N1}_x$ + $\mathbf{N2}_{1-x}$ + **TMDS** + **HD5**] by scrutinizing the variations of ξ and S (Figure 6 and Table 2). In the SmC phase, the evolution of ξ trivially agrees with long-range correlations (25−30 nm), but the transition to the N phase only causes a drop to about half its length, preceding a gradual decrease in the N domain. This differs from the classical behavior of calamitic mesogens,[42] with the immediate collapse of ξ to short range at the transition to the N phase. The variation of S is even more unconventional: instead, as anticipated, of a continuous decrease in the N phase, and the final vanishing at the transition to the isotropic state, S remains constantly large in the N domain and progressively decreases close to and above the transition to the isotropic state. Measurable orientations are still observed at higher temperatures, far beyond the transition to the isotropic state, an indication that the material is maintained in some sort of intermediate transitory state, clearly not a kinetic but a real thermodynamic state, between the nematic

dx.doi.org/10.1021/ma501164u | Macromolecules 2014, 47, 5198−5210

Table 2. Structural Data of the Disiloxane (SmC and N) and Trisiloxane (SmC) Co-Elastomers, [$N1_x$ + $N2_{1-x}$ + TMDS + HD5] and [$N1_x$ + $N2_{1-x}$ + HMTS + HD5] (4 mol % HD5)[a]

elastomers	mesophase	d	ψ_{chev}	ξ [n]	S	h_{si}	h_{mes} + h_{ch}
[$N1_{0.25}$ + $N2_{0.75}$ + TMDS + HD5]	SmC	25.5	41.5	30 [12]	0.90	6.5	4.5
	N	27	49	11 [4]	0.89	n.d	4.5
[$N1_{0.50}$ + $N2_{0.50}$ + TMDS + HD5]	SmC	24.6	40	>60 [>25]	0.91	6.6	4.4
	N	28	44	12 [4]	0.80	n.d.	4.6
[$N1_{0.75}$ + $N2_{0.25}$ + TMDS + HD5]	SmC	26.5	43	26 [10]	0.91	6.8	4.5
	N	27	45	12 [4]	0.90	n.d.	4.5
[N2 + HMTS + HD5]	SmC	26.9	30	30 [11]	0.83	6.6	4.6
[$N1_{0.25}$ + $N2_{0.75}$ + HMTS + HD5]	SmC	28.1	32	24 [9]	0.89	6.8	4.6
[$N1_{0.50}$ + $N2_{0.50}$ + HMTS + HD5]	SmC	28.5	26	34 [12]	0.75	6.8	4.6
[$N1_{0.75}$ + $N2_{0.25}$ + HMTS + HD5]	SmC	28.0	37.5	29 [10]	0.80	6.7	4.6
[N1 + HMTS + HD5]	SmC	28.6	39	29 [10]	n.d.	6.7	4.6

[a]Structural data measured at 25 °C, in the SmC phase and at T = 65, 68, and 85 °C, respectively, in the N phase: d, layer spacing (Å); ψ_{chev}, chevron tilt angle (deg); ξ: correlation length (nm); n: number of correlated layers; S: nematic order parameter; h_{si}, h_{mes} + h_{ch}: scattering maxima for lateral distances between siloxane units, monomers and chains, respectively (Å). n.d.: not determined due to weak signal.

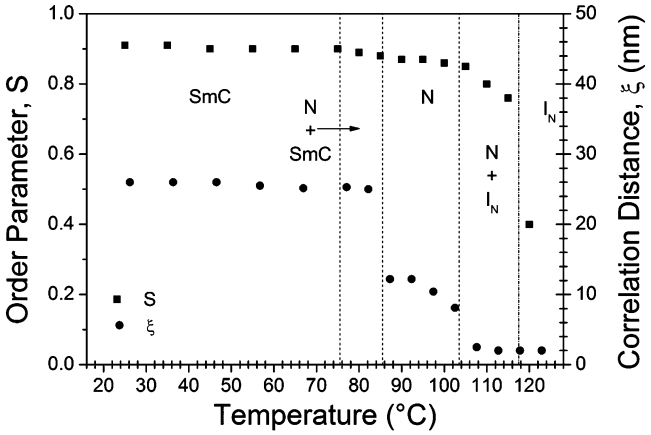

Figure 6. Temperature variations of the order parameter, S, and of the correlation length of smectic layers, ξ, for the co-elastomer [$N1_{0.75}$ + $N2_{0.25}$ + TMDS + HD5], chosen as a representative case. I_N: paranematic-like state state; SmC + N, N + I_N: coexistence regions.

and the isotropic liquid, referred to as paranematic-like state. Clarifying the real nature of such a state would require extensive phase transition studies far beyond the scope of this investigation.[43] Thereafter, the term "paranematic-like" state will be used and labeled as I_N.

The residual orientational order is obviously the main reason for the recovery of the oriented SAXS patterns on cooling and for the delay of the transitions to higher temperatures as in the polymers. The trend observed with the **HMTS** elastomers contrasts sharply with this thermal behavior, as their transitions to the isotropic state are not delayed and erase definitively the orientation of the smectic domains. This behavior would a priori be consistent with classical transitions to isotropic states, thereafter labeled "I".

Therefore, the reticulation of the polymeric chains only modifies slightly the polymorphism: the **HMTS** elastomers mainly display a SmC phase, over almost identical temperature ranges as the nonreticulated systems, and both N and SmC phases are preserved in the **TMDS** systems. However, the network drastically affects the phase transition process, with very different behaviors within both series: reversible changes preserving the memory of the secondary orientation for the **TMDS** systems and irreversible tendencies to return to the initial unoriented state for the **HMTS** systems.

To understand further the relationship with the siloxane spacer, the nanosegregation process needs to be more deeply investigated by accessing to the bulkiness of the different species, especially their partial volumes and cross sections, obtained from reference dilatometric measurements. The individual cross section of mesogens, σ_{mes}, aliphatic chains, σ_{ch}, and siloxane units, σ_{si}, can then be compared to the molecular area A_{mol}, assimilated to the statistical layer portion covered by a single repeat unit, defined as ratio between the repeat unit volume, V_{mol}, and the measured layer spacing, d.[44] The main discrepancy in these systems lies between the cross sections of siloxane ($\sigma_{si} \approx 45$ Å^2) and of the other constitutive moieties ($\sigma_{ch} \approx 21.3$ Å^2, $\sigma_{mesN2} \approx 23.6$ Å^2, and $\sigma_{mesN1} \approx 26.5$ Å^2). The effective molecular areas of the polymers and elastomers take intermediate values, ranging from 32 to 40 Å^2, and involve several compensation mechanisms. The accommodation of the bulky siloxane segments is possible through the ruffling of their sublayers,[45] which occurs more easily with thinner sublayers and hampered by the network, in consistency with the experimental variation of A_{mol} between both series (Table 3). Molecular areas remain however close to siloxane, as the other sublayers more easily expand, through the folding of alkyl chains and the tilting of mesogens.

The ratio σ_{mes}/A_{mol} gives access to the tilt angle, ψ_{mes}, representing the average polar tilt angle of the mesogen axis from the layer normal. This information is completed by the chevron angle, ψ_{chev}, which is directly measured on the oriented SAXS patterns and corresponds to the cone distribution of the smectic layers normal or to the piling direction in the smectic correlation volumes of the nematic phase (Figure 7). The cone axis coincides with the direction of elongation and therefore with the preferential direction of the axes of the polymer chains and of the mesogens. Both tilt angles may be different since they do not relate at the same scale: ψ_{chev} is the macroscopically emerging tilt and possibly integrates an azimuthal distribution of mesogens' axes, while ψ_{mes} refers to the local packing within layers and thus sets the upper limit of ψ_{chev}. The sharpness of the small-angle spots and the closeness of both tilt angles in the **TMDS** elastomers (Figure 4 and Table 3) confirm the uniform mesogen alignment. The tilting is moreover preserved in the N phase within smectic-like clusters (Table 2), the slightly higher angles having different interpretations (thermal expansion, small azimuthal component, etc.). The **HMTS** elastomers show on the contrary a clear gap from ψ_{chev} to ψ_{mes}, without the

dx.doi.org/10.1021/ma501164u | Macromolecules 2014, 47, 5198−5210

Table 3. Structural Data of Polymers and Elastomers in the SmC Phase at 25 °C[a]

polymers/ elastomers	V_{mol} (Å^3)	d (Å)	ψ_{chev} (deg)	A_{mol} (Å^2)	σ_{mes} (Å^2)	ψ_{mes} (deg)	$\Delta\psi$ (deg)
[**N2** + **TMDS**]$_p$	849				23.6		
[**N1**$_{0.25}$ + **N2**$_{0.75}$ + **TMDS**]$_p$	894	27.6		32.4	24.3	41	
[**N1**$_{0.50}$ + **N2**$_{0.50}$ + **TMDS**]$_p$	939	27.6		34.0	25.1	42.5	
[**N1**$_{0.75}$ + **N2**$_{0.25}$ + **TMDS**]$_p$	984	28.5		34.5	25.8	42	
[**N1** + **TMDS**]$_p$	1029				26.5		
[**N2** + **TMDS** + **HD5**]	843*				23.6		
[**N1**$_{0.25}$ + **N2**$_{0.75}$ + **TMDS** + **HD5**]	889	25.5	42	34.9	24.3	46	4
[**N1**$_{0.50}$ + **N2**$_{0.50}$ + **TMDS** + **HD5**]	934	24.6	40	38	25.1	49	9
[**N1**$_{0.75}$ + **N2**$_{0.25}$ + **TMDS** + **HD5**]	979	26.5	43	36.9	25.8	46	3
[**N1** + **TMDS** + **HD5**]	1023*				26.5		
[**N2** + **HMTS**]$_p$	974	28.3		34.4	23.6	47	
[**N1**$_{0.25}$ + **N2**$_{0.75}$ + **HMTS**]$_p$	1019	28.6		35.6	24.3	47	
[**N1**$_{0.50}$ + **N2**$_{0.50}$ + **HMTS**]$_p$	1064	28.5		37.3	25.1	48	
[**N1**$_{0.75}$ + **N2**$_{0.25}$ + **HMTS**]$_p$	1109	29.0		38.3	25.8	48	
[**N1** + **HMTS**]$_p$	1154	29.7		38.9	26.5	47	
[**N2** + **HMTS** + **HD5**]	957	26.9	30	35.6	23.6	48.5	18.5
[**N1**$_{0.25}$ + **N2**$_{0.75}$ + **HMTS** + **HD5**]	1002	28.1	32	35.7	24.3	47	15
[**N1**$_{0.50}$ + **N2**$_{0.50}$ + **HMTS** + **HD5**]	1047	28.5	26	36.7	25.1	47	21
[**N1**$_{0.75}$ + **N2**$_{0.25}$ + **HMTS** + **HD5**]	1092	28.0	38	39.0	25.8	49	21
[**N1** + **HMTS** + **HD5**]	1137	28.6	39	39.8	26.5	48	9

[a]Partial molecular volumes at 25 °C: V_{mol} is the volume of the molecular motif, $V_{mol} = xV_{N1} + (1 - x)V_{N2} + V_{HMTS/TMDS}$ for the polymers, $V_{mol} = xV_{N1} + (1 - x)V_{N2} + 0.9V_{HMTS/TMDS} + 0.04V_{HD5}$ (*$V_{mol} = xV_{N1} + (1 - x)V_{N2} + 0.88V_{HMTS/TMDS} + 0.05V_{HD5}$) for the elastomers; $V_{N1} = 813$ Å^3, $V_{N2} = 633$ Å^3, $V_{TMDS} = 216$ Å^3 (polymers), $V_{TMDS} = 195$ Å^3 (elastomers), $V_{HMTS} = 342$ Å^3 (polymers), $V_{HMTS} = 307$ Å^3 (elastomers), $V_{HD5} = 421$ Å^3. Other structural data: d, layer spacing; $A_{mol} = V_{mol}/d$, molecular area; σ_{N1}, σ_{N2}, cross sections of mesogens **N1** and **N2**, respectively; $\sigma_{mes} = x\sigma_{N1} + (1 - x)\sigma_{N2}$, average cross-section; $\psi_{mes} = \arccos(\sigma_{mes}/A_{mol})$, ψ_{chev}, $\Delta\psi = \psi_{mes} - \psi_{chev}$, mesogen tilt angle, chevron tilt angle and difference.

broadening of the small-angle spots (Figure 5 and Table 3). This means that the orientations of the mesogens deviate from one another, but that the preferential orientation of the smectic domains is still the direction of elongation. In other words, smaller average tilt angles ψ_{chev} emerge from the contributions of zones with different azimuthal component (Figure 7). The orientation of the mesogens is poorly correlated in the **HMTS** elastomers, and the trend between both series proves to be the expression on the SmC structure of the same feature driving the evolution of the polymorphism: the nanosegregation of the siloxane sublayers isolating successive mesogen sublayers from each other (vide infra). With the further lengthening of the siloxane spacers (increase of the volume fraction), the structure should predictably continue evolving in the same way; the macroscopic tilt might then totally vanish ($\psi_{chev} = 0$ with $\psi_{mes} > 45°$) and yield De Vries-like smectic A phases (Figure 7).[46]

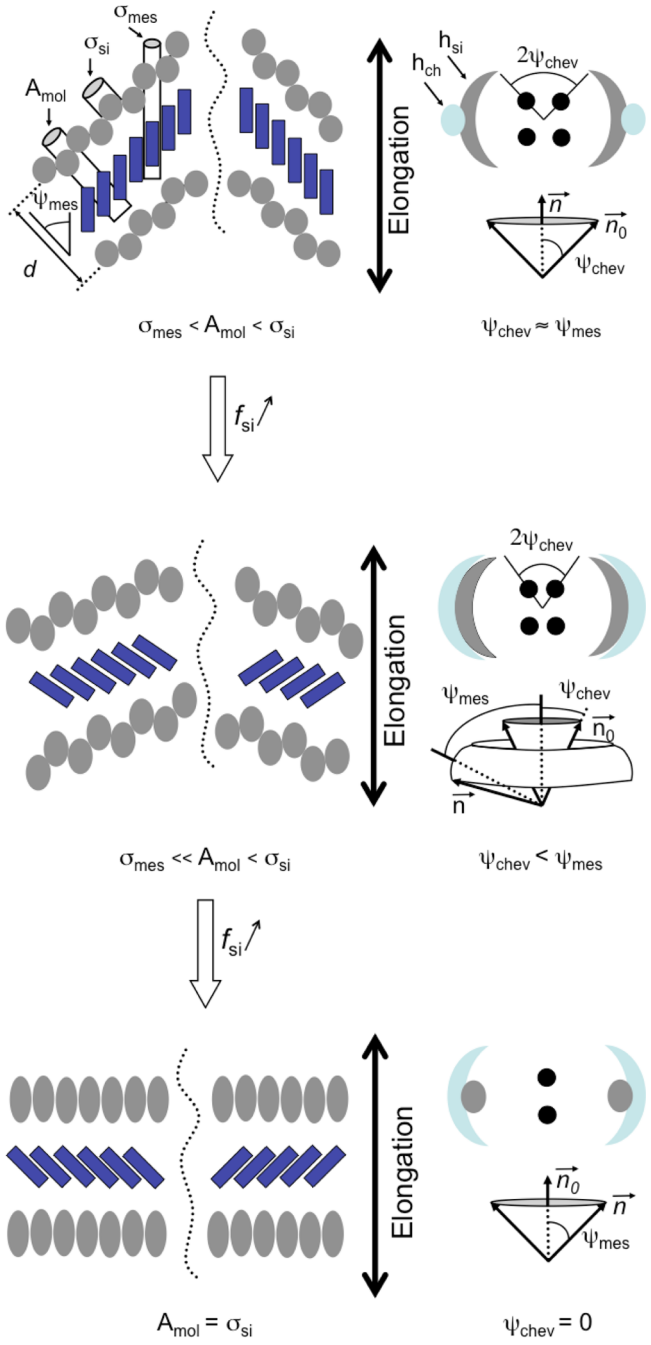

Figure 7. Schematic representations of the molecular packing and corresponding X-ray patterns, in the SmC phase of the stretched elastomers with different lengths of siloxane spacers. Top: **TMDS** spacer. Middle: **HMTS** spacer. Bottom: predictive structure with longer spacer. f_{si} is siloxane volume fraction; $\vec{n}$ and $\vec{n}_0$ represent the directions of the mesogens' axes and of the normal to the layers; ψ_{mes} and ψ_{chev} are the mesogen and the chevron tilt angles; A_{mol} is the molecular area; σ_{si} is the cross section of the siloxane segments.

Corollary, the influence of the siloxane sublayer thickness also provides a molecular interpretation for the observed phase behavior change: the thicker **HMTS** sublayers reduce the correlations between the orientations of the mesogens from successive layers and leave a classical isotropic state when the smectic layers vanish. Conversely, above the broad N ranges of the **TMDS** elastomers, the orientational long-range order is

dx.doi.org/10.1021/ma501164u | Macromolecules 2014, 47, 5198−5210

replaced by residual orientational correlations at a level set by the strength of the cross-linking.

The elastomeric network associates a given structure of cross-linked polymer chains to a shape. The analyses of the phase behavior and of the molecular packing were therefore partially completed with the measurement of the shape variation as a function of temperature for the four following elastomers: [**N1**$_x$ + **N2**$_{1-x}$ + **TMDS** + **HD5**] with x = 0.25 and 0.75 and [**N1**$_x$ + **N2**$_{1-x}$ + **HMTS** + **HD5**] with x = 0 and 0.5. These preliminary thermoelastic experiments were realized with an elongation setup by starting from the "secondary" shape, corresponding to the oriented state fixed during the second preparation step. Measurements were conducted on both heating and cooling cycles by changing the temperature stepwise with 50 min stabilization time at each step. Elongations were calculated in reference to the sample size at the highest measured temperature beyond the mesomorphic range. Data obtained on successive heating and cooling runs for both **TMDS** elastomers superimpose fairly well in the SmC, N, and I_N ranges, except a small hysteresis effect around the N−SmC transition due its first-order character (Figure S16, Supporting Information). The superimposition confirms that the recovery of the secondary orientation in SAXS patterns (vide infra) combines with the recovery of the secondary shape. Consequently, these elastomers exhibit definitively two-way shape-memory effects, obviously in connection with the residual orientational correlations that initiate the growth of the low-temperature oriented states. As for the **HMTS** elastomers, the thermoelastic experiments prove that the definitive erasing of the secondary orientation in the isotropic state underlies the shrinking to a permanent shape close to the initial unoriented state. The lengthening of the siloxane spacer therefore changes the shape-memory behavior for the one-way type. Recall that the cross-linker content is the same in both series of co-elastomers (ca. 1 unit for 25 divalent siloxane units, Tables S6 and S7, Supporting Information), and therefore the density of the cross-linking is unlikely to be at the origin of the switching behavior between both series.

Apart from the reversibility of the shape change on (first) heating, the elastomers differ from one another in their initial elongations and in their rates of shrinking (Figures 8 and 9). Initial elongations lie around 200% for both the **TMDS** co-elastomers and the **HMTS** co-elastomer but reach 350% for the

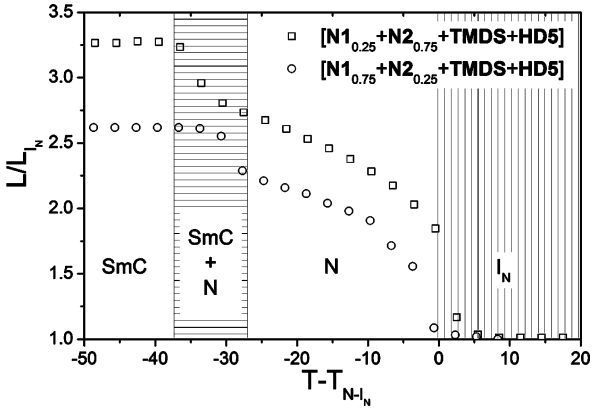

Figure 8. Thermoelastic heating curves of **TMDS** elastomers [**N1**$_x$ + **N2**$_{1-x}$ + **TMDS** + **HD5**], (x = 0.25, 0.75) as a function of the temperature interval to the transition between nematic and para-nematic-like states. SmC + N: coexistence temperature region.

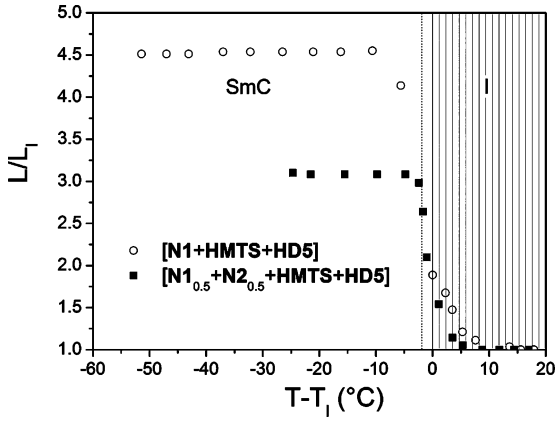

Figure 9. Thermoelastic first heating curves of **HMTS** elastomers, [**N1**$_x$ + **N2**$_{1-x}$ + **HMTS** + **HD5**] (x = 0.50, 1.00) as a function of the temperature interval to the transition between nematic and isotropic states (T_I). The dotted line corresponds to the SmC−N transition of [**N1** + **HMTS** + **HD5**].

HMTS homoelastomer. These values are difficult to interpret as they are influenced by various experimental parameters, such as the exact sample dimensions modified by pinching zones, the elastic properties after the first preparation step depending on the degree of cross-linking, on the relative homogeneity of the network and on the various chain conformations and topologies (opened and closed loops, hairpins, knots, etc.), and on the composition, the polymorphism, and the gap between mesogens and chevron tilt angles, etc. Isolating each influence would be an extensive experimental work far beyond the present study. Whatever the initial elongation, the shape remains constant in the SmC phase; the shrinking always starts a few degrees below the transition to the next phase and ends a few degrees above the transition to the isotropic state. Since the homo-elastomer and the co-elastomer of the **HMTS** series show respectively no and a tiny intermediate N phase, the whole shrinkage takes place abruptly, within a narrow temperature range. To the contrary, the shrinking of the **TMDS** elastomers is gradual and spreads over the broad N range. The rate of shrinking is nevertheless variable, from rather moderate in the middle of the nematic domain, to steep around and inside transitional zones, in connection with the variations of S and ξ deduced from SAXS patterns (vide infra).

To summarize, these prelimary thermoelastic experiments confirm that the reversible X-ray pattern orientations of **TMDS** elastomers effectively underlie the gradual and reversible shape shift throughout the broad nematic range, whereas the once oriented **HMTS** elastomers irreversibly shrink to the unoriented shape as soon as the long-range correlated smectic layers collapse. It should be emphasized that the shape recovery of the **TMDS** elastomers was not affected by the time stayed in the paranematic-like state (up to a day) and that no delay was observed for the irreversible shrinking of the **HTMS** elastomers. Both series of elastomers turned out to be classical soft materials whose properties are determined by the molecular organization.

■ CONCLUSION

A binary system, composed of mesogens with the classical calamitic architecture (rodlike cores of different bulkiness and terminal vinyl−alkyl tails), was incorporated in main-chain polymers via direct hydrosylilation reaction with various linear

dx.doi.org/10.1021/ma501164u | Macromolecules 2014, 47, 5198−5210

siloxane oligomers. Instead of the SmC phase shown by the small monomer, the longer mesogen and all the homogeneous mixtures give rise to broad nematic ranges, consequent to the perturbations of the lateral packing (introduced by the methyl side-group borne by the long mesogen). The nanosegregation of the siloxane spacers confined in intermediate sublayers however counteracts this effect in the resulting alternating polymers, as proven by the emergence of the SmC phase, either below a somewhat shrunken nematic range or with a direct transition to the isotropic state. In addition, the siloxane spacers impose tilt angles close to 45° due to the large difference between the cross sections of both the siloxane fragments and the mesogens.

The mesomorphic properties were marginally affected upon the replacement of a small fraction of the siloxane spacers by cross-linking segments to produce the elastomers. In particular, the room-temperature SmC phase and the subambient glass transition were preserved, which allowed the alignment realized by mechanical elongation during a step of the synthesis and its retention in the final soft material. This alignment provided a deep insight into the intricate structure, especially through the comparison of tilt angle of mesogens and chevron tilt angle of the smectic planes, on the one hand, and through the access to the orientational order parameter and to the smectic correlation length, on the other hand. These detailed structural investigations carried out by SAXS were further completed by a short description of our preliminary thermoelastic experiments, measuring the connected variations of shape.

The length of the siloxane spacer in particular turns out to be an efficient and essential parameter to confer shape-memory behavior of different types to the elastomers, i.e., of the one-way type for the **HMTS** system, for which the elongated shape is erased on heating and not recovered on cooling, and of the two-way type for the **TMDS** system, for which the shape of the samples reversibly changes between states, distinct from the initial shape before the cross-linking step.

For the elastomers with the shorter siloxane spacer, relatively broad nematic ranges were maintained, and strong correlations between the orientations of the mesogens persisted above the mesomorphic range, in consistency with the existence of the paranematic-like state beyond the N phase and with the vanishing gap between mesogens' and chevron tilt angles. These features translated into gradual and reversible variations of elastomers shape with temperature, from constant elongations of about 200% in the SmC phase to almost no elongation in the paranematic-like state. This two-way shape-memory behavior contrasted with the one-way type observed for the other elastomer series with the thicker siloxane sublayers, evidenced by the reduced chevron tilt angle and predominant confinement in sublayers, thus interrupting more efficiently the orientational correlations between mesogens of successive layers. Consistently, the N phase disappeared or was only preserved in a narrow range, while the initial elongations and orientations vanished rapidly and irreversibly close to the transition to the isotropic state. The modifications of the mesogen' orientation and of the sample shape during preparation and thermal treatment necessarily also translate into changes of the entire macromolecular network conformation. Fruitful extensions of this work could be scattering experiments on elastomers with labeled mesogens, NMR spectroscopy, and computational modeling taking into account the mesogens segregation in order to better appreciate the role of the dynamics of the entire network chains conformation on the drastic shape shift.

Therefore, the results obtained in this study appear to be relevant for the designs of shape-memory LC elastomers, with a fairly good anticipation of their elastic and thermal properties. It would also be of interest in future works to extend the variety of spacers to be inserted in the main chain of the polymers to other types of siloxane oligomers of various bulkiness and intricate structures as well as to corresponding mixtures. The use of controlled mixtures of mesogens also proved as an efficient mean to considerably lower the transition temperatures with the partial retention of the mesomorphic behavior of the initial components, and in some cases the survival of the N mesophase. The drastic change between the elastic behaviors (vanishing of the elongated shape memory and of the paranematic-like state between both series) naturally puzzles over the features in the switching zone at intermediate spacer lengths and would merit specific investigations in future works.

■ ASSOCIATED CONTENT

Supporting Information

Experimental part, tables of the thermal behavior of the monomers, copolymers and co-elastomers, selected POM images, DSC traces, SAXS patterns, thermoelastic curves, and centrifuge pictures. This material is available free of charge via the Internet at http://pubs.acs.org.

■ AUTHOR INFORMATION

Corresponding Author

*E-mail Bertrand.Donnio@ipcms.unistra.fr (B.D.).

Notes

The authors declare no competing financial interest.

■ ACKNOWLEDGMENTS

A.G.M., B.H., N.B., D.G., and B.D. thank CONACyT scholarship 185485 for financial funding during this research work (A.G.M.), the European Union through the Research Training Networks project FUNCTIONAL LIQUID-CRYSTALLINE ELASTOMERS (FULCE-HPRN-CT-2002-00169), CNRS, and the Université de Strasbourg for financial support, and Professor Dr. Dr. h.c. Heino Finkelmann for helping in the thermoelastic apparatus and spin-casting centrifuge constructions.

■ REFERENCES

(1) (a) de Gennes, P. G. *Phys. Lett. A* **1969**, *28*, 725−726. (b) de Gennes, P. G. *C. R. Sci. Acad., Ser. B* **1975**, *281*, 101−103.

(2) Finkelmann, H.; Koch, J. H.; Rehage, G. *Makromol. Chem., Rapid Commun.* **1981**, *2*, 317−322.

(3) (a) Finkelmann, H. *Angew. Chem., Int. Ed. Engl.* **1987**, *26*, 816−824. (b) Zentel, R. *Angew. Chem. Adv. Mater.* **1989**, *101*, 1437−1445. (c) Davis, F. J. *J. Mater. Chem.* **1993**, *3*, 551−562. (d) Kelly, S. *J. Mater. Chem.* **1995**, *5*, 2047−2061. (e) Zentel, R.; Brehmer, M. *Acta Polym.* **1996**, *47*, 141−149. (f) Xie, P.; Zhang, R. *J. Mater. Chem.* **2005**, *15*, 2529−2550. (g) Brömmel, F.; Kramer, D.; Finkelmann, H. *Adv. Polym. Sci.* **2012**, *250*, 1−48.

(4) Ohm, C.; Brehmer, M.; Zentel, R. *Adv. Mater.* **2010**, *22*, 3366−3387.

(5) (a) Lendlein, A.; Kelch, S. *Angew. Chem., Int. Ed.* **2002**, *41*, 2034−2057. (b) Liu, C.; Qin, H.; Mather, P. T. *J. Mater. Chem.* **2007**, *17*, 1543−1558. (c) Burke, K. A.; Mather, P. T. *J. Mater. Chem.* **2010**, *20*, 3449−3457. (d) Behl, M.; Zotzmann, J.; Lendlein, A. *Adv. Polym. Sci.* **2010**, *226*, 1−40. (e) Behl, M.; Lendlein, A. *J. Mater. Chem.* **2010**, *20*, 3335−3345. (f) Ahn, S.-k.; Kasi, R. M. *Adv. Funct. Mater.* **2011**, *21*,

4543−4549. (g) Iqbal, D.; Samiullah, M. H. *Materials* **2013**, *6*, 116−142.
(6) (a) Binet, C.; Bourrier, D.; Dilhan, M.; Estève, D.; Ferrère, S.; Garrigue, J.-C.; Granier, H.; Lattes, A.; Gué, A.-M.; Mauzac, M.; Mingotaud, A.-F. *Talanta* **2006**, *69*, 757−762. (b) Jiang, H.; Li, C.; Huang, X. *Nanoscale* **2013**, *5*, 5225−5240.
(7) Sánchez-Ferrer, A.; Fischl, T.; Stubenrauch, M.; Wurmus, H.; Hoffman, M.; Finkelmann, H. *Macromol. Chem. Phys.* **2009**, *210*, 1671−1677.
(8) (a) Knight, D. P.; Volrath, F. *Philos. Trans. R. Soc. London, B* **2002**, *357*, 155−163. (b) Dalhaimer, P.; Discher, D. E.; Lubensky, T. C. *Nat. Phys.* **2007**, *3*, 354−360.
(9) Sungur, E.; Mager, L.; Boeglin, A.; Li, M.-H.; Keller, P.; Dorkenoo, K. D. *Appl. Phys. A: Mater. Sci. Process.* **2010**, *98*, 119−122.
(10) (a) Buguin, A.; Li, M.-H; Silberzan, P.; Ladoux, B.; Keller, P. *J. Am. Chem. Soc.* **2006**, *128*, 1088−1089. (b) Yang, H.; Ye, G.; Wang, X.; Keller, P. *Soft Matter* **2011**, *7*, 815−823.
(11) (a) Ohm, C.; Serra, C.; Zentel, R. *Adv. Mater.* **2009**, *21*, 4859−4862. (b) Ohm, C.; Fleischmann, E.-K.; Kraus, I.; Serra, C.; Zentel, R. *Adv. Funct. Mater.* **2010**, *20*, 4314−4322.
(12) Van Oosten, C. L.; Bastiaansen, C. W. M.; Broer, D. J. *Nat. Mater.* **2009**, *8*, 677−682.
(13) (a) Finkelmann, H.; Nishikawa, E.; Pereira, G. G.; Warner, M. *Phys. Rev. Lett.* **2001**, *87*, 015501. (b) Cviklinski, J.; Tajkbakhsh, A. R.; Terentjev, E. M. *Eur. Phys. J. E* **2002**, *9*, 427−434. (c) Li, M.-H.; Keller, P.; Li, B.; Wang, X.; Brunet, M. *Adv. Mater.* **2003**, *15*, 569−572. (d) Camacho-Lopez, M.; Finkelmann, H.; Palfy-Muhoray, P.; Shelley, M. *Nat. Mater.* **2004**, *3*, 307−310. (e) Beyer, P.; Zentel, R. *Macromol. Rapid Commun.* **2005**, *26*, 874−879. (f) Ikeda, T.; Mamiya, J.; Yu, Y. *Angew. Chem., Int. Ed.* **2007**, *46*, 506−528. (g) Yamada, M.; Kondo, M.; Mamiya, J.-I.; Yu, Y.; Kinoshita, M.; Barrett, C. J.; Ikeda, T. *Angew. Chem., Int. Ed.* **2008**, *47*, 4986−4988. (h) Li, C.; Lo, C.-W.; Zhu, D.; Li, C.; Liu, Y.; Jiang, H. *Macromol. Rapid Commun.* **2009**, *30*, 1928−1935.
(14) (a) Lehmann, W.; Skupin, H.; Tolksdorf, C.; Gebhard, E.; Zentel, R.; Kruger, P.; Losche, M.; Kremer, F. *Nature* **2001**, *410*, 447−450. (b) Courty, S.; Mine, J.; Tajbkhsh, A. R.; Terentjev, E. V. *Europhys. Lett.* **2003**, *64*, 654−660. (c) Yusuf, Y.; Huh, J. H.; Cladis, P. E.; Brand, H. R.; Finkelmann, H.; Kai, S. *Phys. Rev. E* **2005**, *71*, 061702.
(15) Kupfer, J.; Finkelmann, H. *Makromol. Chem., Rapid Commun.* **1991**, *12*, 717−726.
(16) Warner, M.; Terentjev, E. *Liquid Crystalline Elastomers, International Monographs on Physics*; Oxford Science Publications: Oxford, UK, 2003.
(17) Urayama, K. *Macromolecules* **2007**, *40*, 2277−2288.
(18) Skačej, G.; Zannoni, C. *Soft Matter* **2011**, *7*, 9983−9991.
(19) Hanus, K. H.; Pechhold, W.; Soergel, F.; Stoll, B.; Zentel, R. *Colloid Polym. Sci.* **1990**, *268*, 222−229.
(20) Bergmann, G. H. F.; Finkelmann, H.; Percec, V.; Zhao, M. *Macromol. Rapid Commun.* **1997**, *18*, 353−360.
(21) (a) Giamberini, M.; Amendola, E.; Carfagna, C. *Macromol. Chem. Phys.* **1997**, *198*, 3185−3196. (b) Ambrogi, V.; Giamberini, M.; Cerruti, P.; Pucci, P.; Menna, N.; Mascolo, R.; Carfagna, C. *Polymer* **2005**, *46*, 2105−2121. (c) Ribera, D.; Giamberini, M.; Serra, A.; Mantecón, A. *J. Polym. Sci., Part A: Polym. Chem.* **2006**, *44*, 6270−6286.
(22) (a) Ortiz, C.; Wagner, M.; Bhargava, N.; Ober, C. K.; Kramer, E. J. *Macromolecules* **1998**, *31*, 8531−8539. (b) Ortiz, C.; Ober, C. K.; Kramer, E. J. *Polymer* **1998**, *39*, 3713−3718.
(23) (a) Di Maio, L.; Iannelli, P.; Pragliola, S.; Roviello, A.; Sirigu, A. *J. Polym. Sci., Part B: Polym. Phys.* **1998**, *36*, 433−438. (b) Caruso, U.; Hatfull, L.; Roviello, A.; Sirigu, A. *Polymer* **1999**, *40*, 6753−6760.
(24) (a) Tokita, M.; Tagawa, H.; Niwano, H.; Osada, K.; Watanabe, J. *Jpn. J. Appl. Phys. A* **2006**, *45*, 1729−1733. (b) Ishige, R.; Osada, K.; Takagawa, H.; Niwano, H.; Tokita, M.; Watanabe, J. *Macromolecules* **2008**, *41*, 7566−7570. (c) Hiraoka, K.; Tashiro, T.; Tokita, M.; Watanabe, J. *Liq. Cryst.* **2009**, *36*, 115−122. (d) Tashiro, T.; Kondo, Y.; Hiraoka, K. *Macromol. Rapid Commun.* **2010**, *31*, 1948−1953.
(25) (a) Beyer, P.; Terentjev, E. M.; Zentel, R. *Macromol. Rapid Commun.* **2007**, *28*, 1485−1490. (b) Beyer, P.; Braun, L.; Zentel, R. *Macromol. Chem. Phys.* **2007**, *208*, 2439−2448. (c) Ohm, C.; Morys, M.; Forst, R. F.; Braun, L.; Eremin, A.; Serra, C.; Stannarius, R.; Zentel, R. *Soft Matter* **2011**, *7*, 3730−3734. (d) Haseloh, S.; Ohm, C.; Smallwood, F.; Zentel, R. *Macromol. Rapid Commun.* **2011**, *32*, 88−93.
(26) (a) Krause, S.; Dersch, R.; Wendorff, J.; Greiner, A.; Finkelmann, H. *Macromol. Rapid Commun.* **2007**, *28*, 2062−2068. (b) Ishige, R.; Tokita, M.; Naito, Y.; Zhang, C. Y.; Watanabe, J. *Macromolecules* **2008**, *41*, 2671−2676. (c) Malucelli, G.; Iannelli, P.; Giamberini, M. *Polymer* **2009**, *50*, 1948−1956.
(27) Yang, H.; Buguin, A.; Taulemesse, J.-M.; Kaneko, K.; Mery, S.; Bergeret, A.; Keller, P. *J. Am. Chem. Soc.* **2009**, *131*, 15000−15004.
(28) Qin, H.; Mather, P. T. *Macromolecules* **2009**, *42*, 273−280.
(29) Donnio, B.; Wermter, H.; Finkelmann, H. *Macromolecules* **2000**, *33*, 7724−7730.
(30) Aguilera, C.; Bartulin, J.; Hisgen, B.; Ringsdorf, H. *Makromol. Chem.* **1983**, *184*, 253−262.
(31) (a) Rousseau, I.; Qin, H.; Mather, P. T. *J. Am. Chem. Soc.* **2003**, *125*, 15300−15301. (b) Rogez, D.; Brandt, H.; Finkelmann, H.; Martinoty, P. *Macromol. Chem. Phys.* **2006**, *207*, 735−745. (c) de Jeu, W. H.; Obraztsov, E. P.; Ostrovskii, B. I.; Ren, W.; McMullan, P. J.; Griffin, A. C.; Sánchez-Ferrer, A.; Finkelmann, H. *Eur. Phys. J. E* **2007**, *24*, 399−409. (d) Patil, H. P.; Hedden, R. C. *J. Polym. Sci., Part B: Polym. Phys.* **2007**, *45*, 3267−3276. (e) Patil, H. P.; Liao, J.; Hedden, R. C. *Macromolecules* **2007**, *40*, 6206−6216. (f) Bispo, M.; Guillon, D.; Donnio, B.; Finkelmann, H. *Macromolecules* **2008**, *41*, 3098−3110. (g) Ren, W.; McMullan, P. J.; Guo, H.; Kumar, S.; Griffin, A. C. *Macromol. Chem. Phys.* **2008**, *209*, 272−278. (h) Ren, W.; McMullan, P. J.; Griffin, A. C. *Macromol. Chem. Phys.* **2008**, *209*, 1896−1899. (i) Patil, H. P.; Lentz, D. M.; Hedden, R. C. *Macromolecules* **2009**, *42*, 3525−3531. (j) Ren, W.; McMullan, P.-J.; Griffin, A.-C. *Phys. Status Solidi B* **2009**, *246*, 2124−2130. (k) Krause, S.; Zander, F.; Bergmann, G.; Brandt, H.; Wertmer, H.; Finkelmann, H. *C. R. Chim.* **2009**, *12*, 85−104. (l) Zander, F.; Finkelmann, H. *Macromol. Chem. Phys.* **2010**, *211*, 1167−1176. (m) Heinze, P.; Finkelmann, H. *Macromolecules* **2010**, *43*, 6655−6665. (n) Papadopoulos, P.; Heinze, P.; Finkelmann, H.; Kremer, F. *Macromolecules* **2010**, *43*, 6666−6670. (o) Kossack, W.; Papadopoulos, P.; Heinze, P.; Finkelmann, H.; Kremer, F. *Macromolecules* **2010**, *43*, 7532−7539. (p) Lentz, D. M.; Chen, H.; Yu, Z.; Patil, H. P.; Crane, C. A.; Hedden, R. C. *J. Polym. Sci., Part B: Polym. Phys.* **2011**, *49*, 591−598. (q) Ren, W.; Kline, W. M.; McMullan, P. J.; Griffin, A. C. *Phys. Status Solidi B* **2011**, *248*, 105−110. (r) Amela-Cortés, M.; Bruce, D. W.; Evans, K. E.; Smith, C. W. *J. Mater. Chem.* **2011**, *21*, 8436−8442. (s) Amela-Cortés, M.; Heinrich, B.; Donnio, B.; Evans, K. E.; Smith, C. W.; Bruce, D. W. *J. Mater. Chem.* **2011**, *21*, 8427−8435. (t) García-Márquez, A.; Demortière, A.; Heinrich, B.; Guillon, D.; Bégin-Colin, S.; Donnio, B. *J. Mater. Chem.* **2011**, *21*, 8994−8996. (u) Melchert, C.; Behl, M.; Nöchel, U.; Lendlein, A. *Macromol. Mater. Eng.* **2012**, *297*, 1203−1212.
(32) (a) Hashimoto, S.; Yusuf, Y.; Krause, S.; Finkelmann, H.; Cladis, P. E.; Brand, H. R.; Kai, S. *Appl. Phys. Lett.* **2008**, *92*, 181902. (b) Cordoyiannis, G.; Lebar, A.; Rožic, B.; Zalar, B.; Kutnjak, Z.; Žumer, S.; Brömmel, F.; Krause, S.; Finkelmann, H. *Macromolecules* **2009**, *42*, 2069−2073. (c) Cordoyiannis, G.; Sánchez-Ferrer, A.; Finkelmann, H.; Rožič, B.; Žumer, S.; Kutnjak, Z. *Liq. Cryst.* **2010**, *37*, 349−353. (d) Rožič, B.; Krause, S.; Finkelmann, H.; Cordoyiannis, G.; Kutnjak, Z. *Appl. Phys. Lett.* **2010**, *96*, 111901. (e) Sánchez-Ferrer, A.; Finkelmann, H. *Soft Matter* **2013**, *9*, 4621−4627.
(33) de Gennes, P. G. *J. Chem. Phys.* **1971**, *55*, 572−579.
(34) Schleger, P.; Farago, B.; Lartigue, C.; Kollmar, A.; Richter, D. *Phys. Rev. Lett.* **1998**, *81*, 124−127.
(35) Ren, W.; Griffin, A. C. *Phys. Status Solidi B* **2012**, *249*, 1379−1385.
(36) Legge, C. H.; Davis, F. J.; Mitchell, G. R. *J. Phys. (Paris)* **1991**, *1*, 1253−1261.
(37) Ricardo Bispo, M. A. PhD Thesis, 2006, University of Strasbourg, France (http://scd-theses.u-strasbg.fr/1238/).

(38) Sánchez-Ferrer, A.; Finkelmann, H. *Macromolecules* **2008**, *41*, 970−980.
(39) (a) Weissflog, W.; Demus, D. *Cryst. Res. Technol.* **1983**, *18*, 21−24. (b) Weissflog, W.; Demus, D. *Cryst. Res. Technol.* **1984**, *19*, 55−64.
(40) This method was successfully applied in the determination of the average ratio of monomers in liquid-crystalline co-dendrimers: Rueff, J. M.; Barbera, J.; Donnio, B.; Guillon, D.; Marcos, M.; Serrano, J.-L. *Macromolecules* **2003**, *36*, 8368−8375.
(41) (a) Skoulios, A.; Guillon, D. *Mol. Cryst. Liq. Cryst.* **1988**, *165*, 317−332. (b) Tschierske, C. *J. Mater. Chem.* **1998**, *8*, 1485−1508.
(42) (a) Dianoux, A. J.; Volino, F. *J. Phys. (Paris)* **1979**, *40*, 181−190. (b) Scherrel, P. L.; Crellin, D. A. *J. Phys. C3* **1979**, *40*, 211−215.
(43) Cordoyiannis, G.; Lebar, A.; Zalar, B.; Zumer, S.; Finkelmann, H.; Kutnjak, Z. *Phys. Rev. Lett.* **2007**, *99*, 197801.
(44) For example: de Gracia Lux, C.; Donnio, B.; Heinrich, B.; Krafft, M.-P. *Langmuir* **2013**, *29*, 5325−5336.
(45) Fouchet, J.; Douce, L.; Heinrich, B.; Welter, R.; Louati, A. *Beilstein J. Org. Chem.* **2009**, *5*, No. 51.
(46) Lagerwall, J. P. F.; Giesselmann, F. *ChemPhysChem* **2006**, *7*, 20−45.